

Low-Energy Excitations and Ground State Selection in Quantum Breathing Pyrochlore Antiferromagnet $\text{Ba}_3\text{Yb}_2\text{Zn}_5\text{O}_{11}$

T. Haku,¹ K. Kimura,² Y. Matsumoto,¹ M. Soda,¹ M. Sera,² D. Yu,³ R. A. Mole,³ T. Takeuchi,⁴ S. Nakatsuji,¹ Y. Kono,¹ T. Sakakibara,¹ L.-J. Chang,⁵ and T. Masuda¹

¹ *Institute for Solid State Physics, The University of Tokyo, Kashiwa, Chiba 277-8581, Japan*

² *Division of Materials Physics, Graduate School of Engineering Science, Osaka University, Toyonaka, Osaka 560-8531, Japan*

³ *Bragg Institute, Australian Nuclear Science and Technology Organization, Lucas Heights, New South Wales 2234, Australia*

⁴ *Low Temperature Center, Osaka University, Toyonaka, Osaka 560-0043, Japan*

⁵ *Department of Physics, National Cheng Kung University, Tainan 70101, Taiwan*

(Dated: May 30, 2016)

We study low energy excitations in the quantum breathing pyrochlore antiferromagnet $\text{Ba}_3\text{Yb}_2\text{Zn}_5\text{O}_{11}$ by combination of inelastic neutron scattering (INS) and thermodynamical properties measurements. The INS spectra are quantitatively explained by spin-1/2 single-tetrahedron model having XXZ anisotropy and Dzyaloshinskii-Moriya interaction. This model has a two-fold degeneracy of the lowest-energy state per tetrahedron and well reproduces the magnetization curve at 0.5 K and heat capacity above 1.5 K. At lower temperatures, however, we observe a broad maximum in the heat capacity around 63 mK, demonstrating that a unique quantum ground state is selected due to extra perturbations with energy scale smaller than the instrumental resolution of INS.

In geometrically frustrated magnet, a macroscopic degeneracy remains in the ground state at zero temperature, as long as the geometry is preserved. Such a situation contradicts the third law of thermodynamics and small perturbations, which can induce non-trivial quantum states, play an important role in avoiding the breakdown of the basic law^{1,2}. A classic example of the violation of the third law is given by a regular tetrahedron of $S = 1/2$ Heisenberg spins; this has a nonmagnetic ground state with a two-fold degeneracy. In nature, however, neither perfect isolation nor absence of coupling to other degrees of freedom is achieved and a non-degenerate state is induced by a perturbation. In the presence of spin-lattice coupling the lifting of the degeneracy is accompanied by the distortion of the tetrahedron, which is called the spin Jahn-Teller effect³. In the case of a three-dimensional (3D) lattice of corner sharing tetrahedra, i.e., the pyrochlore lattice^{3,4}, the distortion is cooperatively propagated over the crystal, causing a magnetostructural phase transition^{5,6}. For an isolated regular tetrahedral system, on the other hand, experimental study is rare for lack of model compound. The search for a simple and isolated system is a challenge to the third law, leading to discovery of new state of matter at very low temperatures.

In the absence of spin-lattice coupling in the Heisenberg spin pyrochlore system the degeneracy is lifted by 3D spin coupling of the magnetic ground state. This leads to quantum spin liquid⁷, ordering of spin singlet state^{8,9}, or chiral order state^{10,11}. The breathing pyrochlore lattice, i.e., one consisting of arrays of alternating large and small tetrahedra, has been found for the $S = 3/2$ spinels LiACr_4O_8 ($A = \text{In}$ and Ga)^{12,13}. The lattice is an experimental realization of a theoretical perturbation expansion method used for the pyrochlore lattice^{7,8,10}. Theory predicts a spin liquid ground state for this model¹⁴; however, $\text{LiInCr}_4\text{O}_8$ ¹³ exhibits a magnetostructural transition due to the spin Jahn-Teller effect similar to that observed in conventional pyrochlore compounds^{5,6,15–17}. Thus the material that preserves the breathing pyrochlore geometry at low temperature will be important.

$\text{Ba}_3\text{Yb}_2\text{Zn}_5\text{O}_{11}$ is an experimental realization of a breath-

ing pyrochlore lattice formed by Yb^{3+} ions¹⁸, with both the small and large tetrahedra being regular. The oxygen ions surrounding the Yb^{3+} ions are shared by the neighboring Yb^{3+} ions in the small tetrahedra, while those are not shared in the large tetrahedra. This results in the small tetrahedra of Yb_4O_{16} being surrounded by $\text{Zn}_{10}\text{O}_{20}$ supertetrahedra. This crystal structure suggests that intertetrahedra interaction is small and local distortion in the small tetrahedron, if it appears at low temperature, does not propagate to neighboring small tetrahedron. The magnetic susceptibility has been reported and can be explained by an $S = 1/2$ tetrahedron model; no phase transitions were observed with $T \geq 0.38$ K¹⁸. Crystalline electric field (CEF) excitations have been measured by inelastic neutron scattering (INS)¹⁹; the data were explained by four Kramers doublets with a first eigenenergy of 38.2 meV. This means that the low energy excitations are dominated by the ground state doublet and the effective spin 1/2 is a good approximation. Furthermore the eigenfunction of the ground state was shown to exhibit an easy-plane type magnetic moment. Even including this anisotropy term the ground state of the tetrahedral spin system is a doublet in the absence of any intertetrahedron interaction or spin-lattice coupling. As such $\text{Ba}_3\text{Yb}_2\text{Zn}_5\text{O}_{11}$ is a candidate for the classic example of frustrated magnets. In this communication we study low energy excitations to identify the effective spin Hamiltonian by INS experiment and macroscopic properties at very low temperatures to see how nature keeps the third law of thermodynamics. We demonstrate how the degeneracy of the ground state is lifted and unique quantum state is selected in $\text{Ba}_3\text{Yb}_2\text{Zn}_5\text{O}_{11}$.

INS experiments were performed using the neutron spectrometer PELICAN²⁰ at ANSTO. We utilized setup I using an incident energy E_i of 2.1 meV and setup II using an E_i of 3.6 meV. Setup I afforded a resolution of 0.059 meV full width half maximum (FWHM) at the elastic line, while setup II gave 0.135 meV.

The INS spectra measured using setup I are shown in Figs. 1(a)-1(d). Three flat bands are observed at 1.5 K; the absence of dispersion suggests that these bands are approxi-

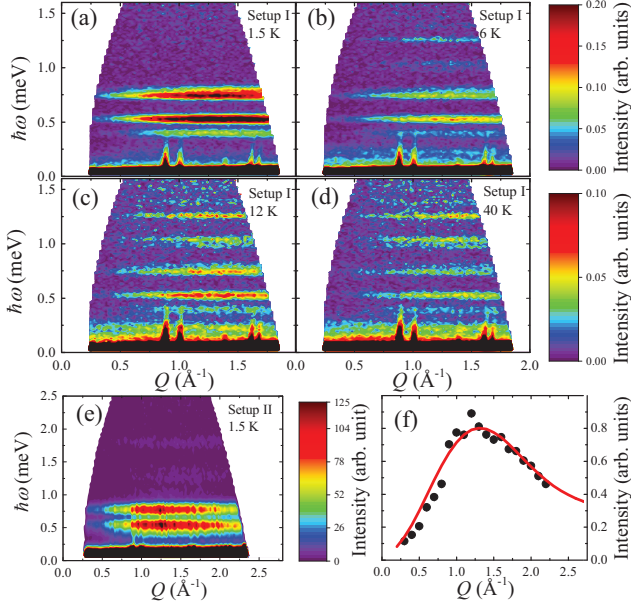


FIG. 1: (a)-(d) INS spectra measured at 1.5 K (a), 6 K (b), 12 K (c), and 40 K (d) using setup I. (e) INS spectrum measured at 1.5 K using the setup II. (f) Q dependence of the integrated intensity obtained from spectrum in (e). Red solid curve is the calculation (see text).

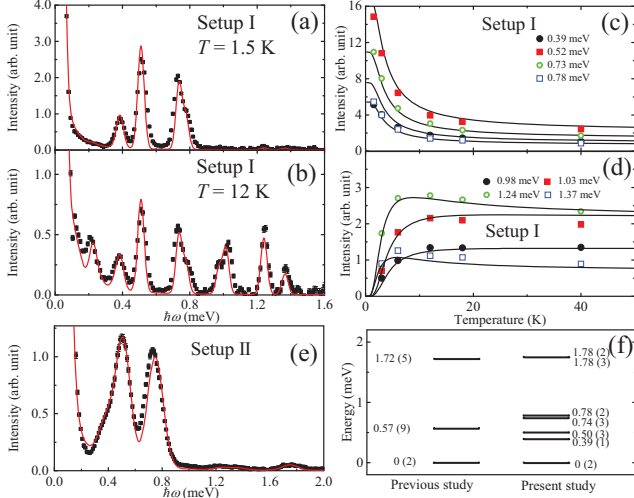


FIG. 2: (a), (b) The $\hbar\omega$ dependences of the neutron intensities at 1.5 K for (a) and 12 K for (b). (c) Temperature dependences of the intensities of the excitations in (a). (d) Those of the excitations additionally observed in high temperatures in (b). (e) $\hbar\omega$ dependence of the intensity at 1.5 K obtained using setup II. Throughout the panels red and black solid curves are the calculation using the same parameters in Eqs. (3)-(6). (f) Energy level of $S = 1/2$ Heisenberg spin tetrahedron model in the previous study¹⁸ and that of $S = 1/2$ anisotropic spin tetrahedron in the present study.

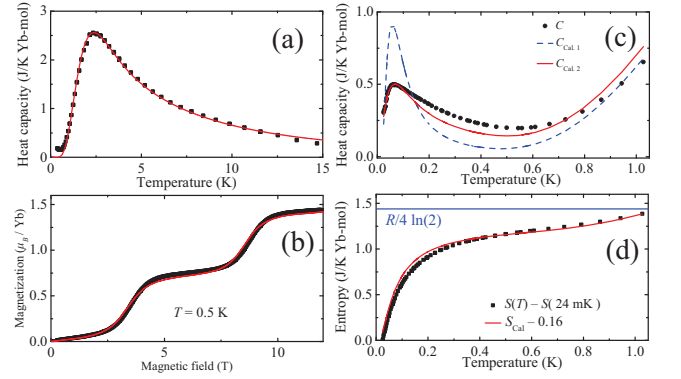


FIG. 3: (a) Heat capacity measured reported in the previous study¹⁸. Red solid curve is calculation. (b) Magnetic field dependence of magnetization at 0.5 K. Red solid curve is calculation. (c) Filled circles indicate heat capacity. Blue dashed curve is the calculation of the empirical model where the lift of the degeneracy of the ground state is introduced as a single energy gap. Red solid curve is the calculation of the model where the empirical energy gap has distribution. (d) Entropy change estimated from (c). The calculated entropy is shifted so that the calculation has the same value of the data at 0.94 K.

mately cluster excitations and the effect of any intercluster excitation is small and hidden in the instrumental resolution. At 6 K the intensities of these three excitations are suppressed and additional flat bands are observed at different $\hbar\omega$'s. In all panels there are several streaks observed in the range $\hbar\omega \lesssim 0.4$ meV which was ascribed to acoustic phonons. Figure 1(e) shows the INS spectrum obtained using setup II while panel (f) shows the Q dependence of the intensity integrated over the range $0.25 \text{ meV} < \hbar\omega < 0.95 \text{ meV}$.

The symbols in Figs. 2(a) and 2(b) shows the one dimensional energy cuts from the data presented in Figs. 1(a) and 1(c), respectively. The peaks are fitted by Gaussian functions with FWHM restricted to that of instrumental resolution to estimate the peak energies and the intensities. The peak energies at 1.5 K are 0.39, 0.52, 0.73 and 0.78 meV. At 12 K additional peaks are observed in Fig. 2(b). The temperature dependence of the four excitations observed at 1.5 K are shown in Fig. 2(c), while the additional excitations at 12 K are shown in Fig. 2(d). The former monotonically decrease with increasing temperature while the latter show the opposite behavior. This implies that those excitations at 1.5 K are ground state transitions and those at 12 K originate from excited states.

Figure 2(e) shows one-dimensional energy cuts from the INS spectra at 1.5 K in Fig. 1(e) using setup II. A peak is observed at 1.75 meV in addition to the peaks in setup I. The Q dependence of the intensity in Fig. 1(f) exhibits broad maximum at $Q_{\text{max}} \sim 1.25 \text{\AA}^{-1}$. This means that antiferromagnetic correlation between the spins, the characteristic length scale of which is π/Q_{max} , is enhanced. The dispersionless excitations with the Q dependent intensity means that the neutron spectrum is dominated by an antiferromagnetic cluster within the instrumental resolution.

For analysis on INS spectra we assume a spin tetrahedron

model. The number of the excitations observed at the base temperature is four, which is inconsistent with Heisenberg $S = 1/2$ spin tetrahedron. We, therefore, consider the following general expression²²:

$$\mathcal{H} = - \sum_{i < j} \sum_{\nu\mu} J_{ij}^{\nu\mu} S_i^\nu S_j^\mu. \quad (1)$$

Here i and j are the labels of the spins on the tetrahedron and ν and μ represent Cartesian coordinates x , y , and z which are defined along the crystallographic a , b and c -axes, respectively. The position vectors for the spins are $\mathbf{r}_1 = d/\sqrt{3}(1, 1, 1)$, $\mathbf{r}_2 = d/\sqrt{3}(-1, -1, 1)$, $\mathbf{r}_3 = d/\sqrt{3}(1, -1, -1)$, and $\mathbf{r}_4 = d/\sqrt{3}(-1, 1, -1)$, where $2\sqrt{2}d$ is the length of the side of the tetrahedron. The symmetry of the regular tetrahedron determines the form of the interaction tensor \hat{J}_{ij} ²², for example in the case of \hat{J}_{12} one gets,

$$\hat{J}_{12} = \begin{pmatrix} J_{xx} & J_{yx} & J_{zx} \\ J_{xy} & J_{yy} & J_{zy} \\ J_{xz} & J_{yz} & J_{zz} \end{pmatrix} = \begin{pmatrix} J_1 & J_3 & -J_4 \\ J_3 & J_1 & -J_4 \\ J_4 & J_4 & J_2 \end{pmatrix}. \quad (2)$$

Using the Hamiltonian in Eq. (1) and the interaction tensor \hat{J}_{ij} , we calculate the neutron scattering cross section. We performed a numerical fitting to the peak energies and their intensities measured at $T = 1.5$ K in setup I using a genetic algorithm. The fitting parameters are J_1 , J_2 , J_3 , J_4 and a scale factor. Here J_1 is an XY type interaction, J_2 is Ising type, J_3 is a pseudo-dipole-type and J_4 is Dzyaloshinskii-Moriya (DM) type. The magnitude of the Dzyaloshinskii correspond to $\sqrt{2}J_4$. The best fit parameters are:

$$J_1 = -0.570 \pm 0.033 \text{ meV}, \quad (3)$$

$$J_2 = -0.558 \pm 0.028 \text{ meV}, \quad (4)$$

$$J_3 = 0.000 \pm 0.023 \text{ meV}, \quad (5)$$

$$J_4 = 0.113 \pm 0.014 \text{ meV}. \quad (6)$$

These are consistent within error to those obtained from independent INS experiments reported recently by another group²³. The results show that the system has an easy-plane XXZ type anisotropy with the DM-type interaction about 30 % of the main interaction. The predicted intensities have been convoluted with the instrumental resolution and are indicated by the solid red curves in Figs. 2(a) and 2(b). Similarly the predicted temperature dependence is shown in Figs. 2(c) and 2(d) by the solid black curves. All the data are reproduced by the calculations. The data collected using setup II in Fig. 1(e) is also reproduced using the same set of parameters. Thus we can conclude that the neutron data are explained by $S = 1/2$ spin tetrahedron including DM interaction in the temperature range $1.5 \text{ K} \leq T \leq 40 \text{ K}$.

The energy levels obtained in the INS experiment are shown in right hand panel of Fig. 2(f). The eigenenergies are calculated using the parameters from Eqs. (3)-(6). For reference the energy level obtained by bulk measurements¹⁸ on the basis of Heisenberg model is shown in the left panel. The energy levels of the Heisenberg model is characterized by a total spin $S_{\text{total}} = S_1 + S_2 + S_3 + S_4$. The nine-fold degeneracy of the

first excited state of $S = 1$ is lifted by the XXZ anisotropy and DM interactions. Similarly the degeneracy of the $S = 2$ state is lifted. The doublet of the ground state is, however, lifted neither by the anisotropy nor DM interaction in the framework of isolated tetrahedron Hamiltonian. In the present model, total spin S_{total} is no longer a good quantum number because DM interaction mixes the eigenstates in isotropic Hamiltonian. This modifies the selection rules of neutron scattering and allows finite matrix components for the transitions among all the eigenstates and leads to the observation of many excitations in the INS spectra.

The anisotropic exchange parameters determined using INS was then used to calculate the thermodynamic properties of the Hamiltonian Eq. (1) and a comparison to experiment was made. Figure 3(a) shows the heat capacity calculated using Eq. (1), together with that measured in a previous study¹⁸. The data is reasonably reproduced by the calculation for $T \geq 1.5$ K; a broad peak at $T \sim 2.5$ K indicates the Schottky anomaly associated with the excited states in the range $0.39 \text{ meV} \leq \hbar\omega \leq 0.78 \text{ meV}$ as shown in Fig. 2(f). An excellent agreement between experiment and calculation is also observed for the full magnetization curve at 0.5 K in Fig. 3(b). Here the best reproduction of the data was with an anisotropic g tensors $g_\perp = 2.78$ and $g_\parallel = 2.22$, where the principle axis of the g factor is taken along \hat{r}_i . This easy-plane anisotropy of the g -tensor is consistent with the previous study. The magnetization curve exhibits two pronounced steps at $H_{C1} \sim 3.5$ T and $H_{C2} \sim 8.8$ T; these correspond to the transitions from the doublet ground state to the first set of excited states in the range of $0.39 \text{ meV} \leq \hbar\omega \leq 0.78 \text{ meV}$ and the first set to the second set at $\hbar\omega \sim 1.75 \text{ meV}$ in Fig. 2(f). The effect of the anisotropic exchange interactions manifests in the non-equivalent distance of the steps and the ramp-like structure rather than the stair-like structure. The former are not expected for a Heisenberg spin tetrahedron model. The anisotropic exchange interactions mix the $S_{\text{total}} = 0$ and $S_{\text{total}} = 1$ states, giving rise to a finite magnetic moment of the lowest energy doublet with $\langle S_{\text{total}} \rangle_{\text{GS}} = 0.13$, which is consistent with the finite slope at $H < 2.5$ T.

Thus, the anisotropic $S = 1/2$ single tetrahedral model can account for multiple experimental data: the INS spectra at 1.5 K in the range of $\hbar\omega \gtrsim 0.15 \text{ meV}$, the magnetization curve at 0.5 K, and heat capacity above 1.5 K. However, this model has a two-fold degeneracy of the lowest energy state, from which the real ground state should be selected by additional interactions that are not included in this model. Therefore we performed heat capacity measurements in the range 24 mK to 1 K, the results of this are shown in Fig. 3(c). Rather than a sharp peak indicative of a phase transition, the heat capacity exhibits a broad peak at $T \sim 63$ mK. The entropy change per Yb^{3+} ion is calculated to be $1.4 \text{ J/K} \sim R/4 \ln(2)$; the calculation is shown as the solid line in Fig. 3(d). Such a change in entropy corresponds to the release of two degrees of freedom per spin-tetrahedron. Thus, the heat capacity measurements at low temperature demonstrate that a unique ground state is finally selected from the doublet ground state of the single tetrahedral model.

To explain the heat capacity and entropy change, we firstly

assume that the doublet ground state of all the spin tetrahedra is lifted by a single energy gap E_g . This corresponds to the assumption that all the Yb_4 tetrahedra are uniformly distorted. The dashed curve in Fig. 3(c) is the calculation using $E_g = 0.012$ meV; the calculated heat capacity is dominated by Schottky behavior from the two level system of the split doublet. The peak is much narrower than that of experiment and the model does not explain the data. Secondly, we assume that E_g has distribution, which includes the possibilities of different E_g for each spin tetrahedron and dispersive E_g due to inter-tetrahedra interaction. We use Lorentzian function for the distribution of E_g with the peak center $E_c = 0.010$ meV and the FWHM $E_l = 0.016$ meV. The calculated heat capacity and entropy change are indicated by red solid curves. The calculation reasonably reproduces the data. The doublet ground state of the isolated tetrahedral Hamiltonian identified within the instrumental resolution of INS experiment is, thus, lifted by a perturbation. Furthermore the energy gap exhibits distribution or dispersion.

The ground state of $\text{Ba}_3\text{Yb}_2\text{Zn}_5\text{O}_{11}$ is, therefore, not a solution of the spin Hamiltonian in Eq. (1) but a non-trivial quantum state. The possible perturbations for lifting this degeneracy should be discussed; one possibility is that there is an interaction between spin tetrahedra, although this is small. The theory of Heisenberg spin tetrahedra predicts that a partial ordering is induced and the energy gap is estimated as $10^{-3}J_{\text{inter}}^3/48J_{\text{intra}}^2$ ⁸, where J_{intra} and J_{inter} are the intra and inter tetrahedron interactions, respectively. Since no dispersion is observed within the instrumental resolution of 0.059 meV we can assume that the band width of the excitations is smaller than this value. This leads to the estimation of an upper bound for J_{inter} of 0.015 meV using the RPA approximation. Note that $J_{\text{intra}} \sim 0.5$ meV in Eq. (3), and the magnitude of the calculated gap is too small to explain the observed gap. However a large asymmetric interaction, J_4 , is obtained, this is 20% of J_1 and J_2 . The theory considering DM interactions with a magnitude of a few percent of the main Heisenberg interaction suggests that the energy gap of the partial ordering of dimers is qualitatively enhanced²⁶. Furthermore a chiral ordered phase is predicted at lower temperatures. The candidates for the quantum ground state are therefore either a partial ordering of dimers or a chiral ordered state induced by a

combination of inter-tetrahedra interactions and a large DM interaction.

Another possibility for the perturbation is spin lattice coupling. In a single spin $S = 1/2$ tetrahedron coupled to the lattice, the ground state doublet is lifted by the spin Jahn-Teller (JT) mechanism³. In the spinel compounds ZnV_2O_4 and MgV_2O_4 ^{3,4} a magnetostructural transitions was observed, which was due to a coupling of the interaction pathways and the three dimensional lattice. While in MgCr_2O_4 a precursor to the spin JT was observed above the transition due to the spin dynamical JT (DJT) effect²⁷. In contrast to the uniform array of tetrahedra in the pyrochlore lattice, the Yb_4O_{16} tetrahedra in $\text{Ba}_3\text{Yb}_2\text{Zn}_5\text{O}_{11}$ are surrounded by JT inactive $\text{Zn}_{10}\text{O}_{20}$ supertetradra and are comparatively isolated. This circumstance is quite similar to that in the honeycomb compound $\text{Ba}_3\text{CuSb}_2\text{O}_9$ ^{28,29}, where the Cu^{2+} tetrahedra are face-shared by JT-inactive SbO_6 octahedra and thus isolated; this suppresses the static JT distortion and a quantum spin liquid is induced by DJT^{30,31}. In analogy to $\text{Ba}_3\text{CuSb}_2\text{O}_9$ the spin DJT is a candidate for the microscopic mechanism of the suppression of the structural transition and the appearance of a quantum spin liquid in $\text{Ba}_3\text{Yb}_2\text{Zn}_5\text{O}_{11}$. However, no equivalent theory has been reported for the breathing pyrochlore lattice and the ground state is still an open question.

Acknowledgments

Prof. Tsuyoshi Kimura is greatly appreciated for helpful discussion. T. Haku was supported by the Japan Society for the Promotion of Science through the Program for Leading Graduate Schools (MERIT). This work was supported by JSPS KAKENHI Grant in Aid for Scientific Research (B) Grant No. 24340077 and 24340075. Travel expenses for the experiment performed using PELICAN at ANSTO, Australia, were supported by General User Program for Neutron Scattering Experiments, Institute for Solid State Physics, The University of Tokyo (proposal No. 15543), at JRR-3, Japan Atomic Energy Agency, Tokai, Japan. Magnetization measurement was carried out by the joint research in the Institute for Solid State Physics, the University of Tokyo.

¹ A. P. Ramirez, Annu. Rev. Mater. Sci. **24**, 453 (1994).

² L. Balents, Nature **464**, 199 (2010).

³ Y. Yamashita and K. Ueda, Phys. Rev. Lett. **85**, 4960 (2000).

⁴ O. Tchernyshyov, R. Moessner, and S. L. Sondhi, Phys. Rev. Lett. **88**, 067203 (2002).

⁵ Y. Ueda, N. Fujiwara, and H. Yasuoka, Journal of the Physical Society of Japan **66**(3), 778 (1997).

⁶ H. Mamiya and M. Onoda, Solid State Commun. **95**, 217 (1995).

⁷ B. Canals and C. Lacroix, Phys. Rev. Lett. **80**, 2933 (1998).

⁸ H. Tsunetsugu, Phys. Rev. B **65**, 024415 (2001).

⁹ E. Berg, E. Altman, and A. Auerbach, Phys. Rev. Lett. **90**, 147204 (2003).

¹⁰ J. H. Kim and J. H. Han, Phys. Rev. B **78**, 180410(R) (2008).

¹¹ F. J. Burnell, S. Chakravarty, and S. L. Sondhi, Phys. Rev. B **79**,

144432 (2009).

¹² Y. Okamoto, G. J. Nilsen, J. P. Attfield, and Z. Hiroi, Phys. Rev. Lett. **110**, 097203 (2013).

¹³ G. J. Nilsen, Yoshihiko Okamoto, Takatsugu Masuda, Juan Rodriguez-Carvajal, Hannu Mutka, Thomas Hansen, and Zenji Hiroi, Phys. Rev. B **91**, 174435 (2015).

¹⁴ O. Benton and N. Shannon, J. Phys. Soc. Jpn **84**, 104710 (2015).

¹⁵ S. H. Lee, C. Broholm, T. H. Kim, W. Ratcliff, and S.-W. Cheong, Phys. Rev. Lett. **84**, 3718 (2000).

¹⁶ M. Matsuda, H. Ueda, A. Kikkawa, Y. Tanaka, K. Katsumata, Y. Narumi, T. Inami, Y. Ueda, and S.-H. Lee, Nat. Phys. **3**, 397 (2007).

¹⁷ H. Ueda, H. A. Katori, H. Mitamura, T. Goto, and H. Takagi, Phys. Rev. Lett. **94**, 047202 (2005).

- ¹⁸ K. Kimura, S. Nakatsuji, and T. Kimura, Phys. Rev. B **90**, 060414(R) (2014).
- ¹⁹ T. Haku, M. Soda, M. Sera, K. Kimura, S. Itoh, T. Yokoo, and T. Masuda, Journal of the Physical Society of Japan **85**, 034721 (2016).
- ²⁰ D. Yu, R. Mole, T. Noakes, S. Kennedy, and R. Robinson, Journal of the Physical Society of Japan **82**, SA027 (2013).
- ²¹ T. Sakakibara, H. Mitamura, T. Tayama and H. Amitsuka, Jpn. J. Appl. Phys. **33**, 5067 (1994).
- ²² K. A. Ross, L. Savary, B. D. Gaulin, and L. Balents, Phys. Rev. X **1**, 021002 (2011).
- ²³ J. G. Rau, L. S. Wu, A. F. May, L. Poudel, B. Winn, V. O. Garlea, A. Huq, P. Whitfield, A. E. Taylor, M. D. Lumsden, M. J. P. Gingras, and A. D. Christianson, arXiv:1601.04104.
- ²⁴ G. Squires, *Introduction to the theory of THERMAL NEUTRON SCATTERING* (Cambridge University Press, Cambridge, 2002).
- ²⁵ J. Holland, *Adaptation in Natural and Artificial Systems* (University of Michigan Press, MI, 1975).
- ²⁶ V. N. Kotov, M. Elhajal, M. E. Zhitomirsky, and F. Mila, Phys. Rev. B **72**, 014421 (2005).
- ²⁷ T. Watanabe, S-I. Ishikawa, H. Suzuki, Y. Kousaka, and K. Tomiyasu, Phys. Rev. B **86**, 144413 (2012).
- ²⁸ H. D. Zhou, E.S. Choi, G. Li, L. Balicas, C.R. Wiebe, Y. Qiu, J.R.D. Copley, and J.S. Gardner, Phys. Rev. Lett. **106**, 147204 (2011).
- ²⁹ S. Nakatsuji, K. Kuga, K. Kimura, R. Satake, N. Katayama, E. Nishibori, H. Sawa, R. Ishii, M. Hagiwara, F. Bridges, T. U. Ito, W. Higemoto, Y. Karaki, M. Halim, A. A. Nugroho, J. A. Rodriguez-Rivera, M. A. Green, and C. Broholm, Science **336**, 559 (2012).
- ³⁰ J. Nasu and S. Ishihara, Phys. Rev. B **88**, 094408 (2013).
- ³¹ Y. Han, M. Hagiwara, T. Nakano, Y. Nozue, K. Kimura, M. Halim, and S. Nakatsuji, Phys. Rev. B **92**, 180410(R) (2015).